

Magnetic kagome materials $RETi_3Bi_4$ family with weak interlayer interactions

Jingwen Guo^{1,2#}, Liqin Zhou^{3,4#}, Jianyang Ding^{5#}, Gexing Qu^{3,4}, Zhengtai Liu⁶, Yu Du^{1,2}, Heng Zhang^{1,2}, Jiajun Li^{1,2}, Yiyi Zhang^{1,2}, Fuwei Zhou^{1,2}, Wuyi Qi^{1,2}, Fengyi Guo^{1,2}, Tianqi Wang^{1,2}, Fucong Fei^{1,7,8*}, Yaobo Huang⁶, Tian Qian³, Dawei Shen⁹, Hongming Weng^{3,4,10*}, Fengqi Song^{1,8*}

¹ *National Laboratory of Solid State Microstructures, Collaborative Innovation Center of Advanced Microstructures, Nanjing University, Nanjing 210093, China.*

² *School of Physics, Nanjing University, Nanjing 210093, China.*

³ *Beijing National Laboratory for Condensed Matter Physics, Institute of Physics, Chinese Academy of Sciences, Beijing 100190, China.*

⁴ *University of Chinese Academy of Sciences, Beijing 100049, China.*

⁵ *State Key Laboratory of Functional Materials for Informatics, Shanghai Institute of Microsystem and Information Technology (SIMIT), Chinese Academy of Sciences, Shanghai 200050, China.*

⁶ *Shanghai Synchrotron Radiation Facility, Shanghai Advanced Research Institute, Chinese Academy of Sciences, Shanghai 201210, China.*

⁷ *School of Materials Science and Intelligent Engineering, Nanjing University, Suzhou 215163, China.*

⁸ *Atom Manufacturing Institute, Nanjing 211806, China.*

⁹ *National Synchrotron Radiation Laboratory, University of Science and Technology of China, 230029 Hefei, China.*

¹⁰ *Songshan Lake Materials Laboratory, Dongguan, Guangdong 523808, China.*

These authors contributed equally to this work.

* Corresponding authors. E-mail: feifucong@nju.edu.cn; hmweng@iphy.ac.cn; songfengqi@nju.edu.cn;

Abstract

Kagome materials have attracted a surge of research interest recently, especially for the ones combining with magnetism, and the ones with weak interlayer interactions which can fabricate thin devices. However, kagome materials combining both characters of magnetism and weak interlayer interactions are rare. Here we investigate a new family of titanium based kagome materials $RETi_3Bi_4$ ($RE = Eu, Gd$ and Sm). The flakes of nanometer thickness of $RETi_3Bi_4$ can be obtained by exfoliation due to the weak interlayer interactions. According to magnetic measurements, out-of-plane ferromagnetism, out-of-plane anti-ferromagnetism, and in-plane ferromagnetism are formed for $RE = Eu, Gd$, and Sm respectively. The magnetic orders are simple and the saturation magnetizations can be relatively large since the rare earth elements solely provide the magnetic moments. Further by angle-resolved photoemission spectroscopy (ARPES) and first-principles calculations, the electronic structures of $RETi_3Bi_4$ are investigated. The ARPES results are consistent with the calculations, indicating the bands characteristic with kagome sublattice in $RETi_3Bi_4$. We expect these materials to be promising candidates for observation of the exotic magnetic topological phases and the related topological quantum transport studies.

Introduction

Materials with kagome lattices have been studied for a long time in the condensed matter physics¹⁻⁴. Kagome lattice is made of two-dimensional honeycomb network of corner-sharing triangles⁵. Based on the simple tight-binding model⁶, it can host flat bands, Dirac cones, as well as saddle points, which have been theoretically predicted and experimentally observed⁷⁻¹⁰. Combining with spin-orbit coupling (SOC) and magnetism, plenty of topological phases have been realized in kagome materials and fruitful novel properties have emerged. For example, large intrinsic anomalous Hall effect (AHE) arising from Berry curvature has been observed in Weyl semimetal $\text{Co}_3\text{Sn}_2\text{S}_2$ and nonlinear antiferromagnets Mn_3X ($\text{X} = \text{Sn}, \text{Ge}$)¹¹⁻¹⁵. Flat band and Dirac cones have been discovered in CoSn ^{10,16} and Fe_xSn_y family^{9,17,18}. In recent years, kagome magnet system RT_6X_6 ($\text{R} = \text{rare earth}; \text{T} = \text{V}, \text{Cr}, \text{Mn}, \text{Fe}, \text{Co}; \text{X} = \text{Ge}, \text{Sn}$) with crystallizing in the MgFe_6Ge_6 structure has also attracted immense interest due to the hosted massive Dirac fermions, flat band along with Dirac cones, and the large intrinsic anomalous Hall effect¹⁹⁻²⁶. Although the material candidates with kagome lattices varies, most of their interlayer interactions are strong, which makes the synthesized crystals bulky, and the properties of the kagome layer inside these materials deviate from the raw two-dimensional kagome lattices. The bulky 3D crystals are difficult to fabricate thin film devices on certain substrates and to tune the physical properties of the materials by gate voltage. Therefore, people are focusing on the discovery of kagome materials with weak interlayer interactions. In 2019, a new family materials KV_3Sb_5 , RbV_3Sb_5 , and CsV_3Sb_5 were discovered²⁷. In this family, considering the weak chemical bonds between V, Sb_2 , and alkali metal atoms, the crystals are cleavable by knives or scotch tapes²⁷, and thin flakes can be exfoliated on substrates such as silicon wafers and Al_2O_3 , and mesoscopic transport devices can be fabricated²⁸⁻³⁰. Superconductivity and charge density wave have also been found in this family of materials^{27,31-37}, which has caused great interest of researchers in condensed matter physics and material science. However, comparing with the multiple types of magnetism and the fruitful researches on magnetic topological phases and anomalous Hall effect in kagome materials with strong interlayer interactions such as Fe_3Sn_2 , Mn_3Sn , FeSn , $\text{Co}_3\text{Sn}_2\text{S}_2$, and TbMn_6Sn_6 family, and there is no spontaneous magnetization among these kagome materials of KV_3Sb_5 family with weak interlayer interactions. Therefore, finding a kagome material with weak interlayer interactions which combines magnetism, kagome lattices, cleavable crystals,

and thin film device availability, would greatly benefit the exploration of more kagome physical properties and fruitful magnetic topological phases.

In this work, we investigate a newly discovered kagome materials $RETi_3Bi_4$ ($RE = Eu, Gd, \text{ and } Sm$). In this family, titanium atoms form the kagome lattice. The interlayer interactions between the adjacent RE/Bi layers are weak due to the limited spatial density of the $RE-RE$ zig-zag chain shaped chemical bonds. By mechanical exfoliation by tapes, the crystals of all three materials can be exfoliated into thin films with thickness as low as nanometer scale. The magnetic properties of $RETi_3Bi_4$ family are also systematically measured. Unlike the previously studied Mn or Fe based kagome lattices, the spontaneous magnetization is not provided by kagome lattice itself formed by transition metals, but solely by rare earth elements. Simple magnetism of out-of-plane ferromagnetism (FM), out-of-plane anti-ferromagnetism (AFM), and in-plane ferromagnetism are formed for $RE = Eu, Gd, \text{ and } Sm$ respectively. Combining with the first-principle calculations and angle-resolved photoemission spectroscopy (ARPES), the band structures of this family of compounds are also investigated. We take $EuTi_3Bi_4$ as the representative to elucidate the exotic electronic properties of these materials with kagome sublattices. We observed the distinct bands with Dirac cone-like dispersions and the flat bands above the Fermi level by calculation, and the ARPES results are consistent with the calculations for the band dispersions below Fermi energy. $RETi_3Bi_4$ family of kagome compounds combines cleavable lattice structure and tunable but simple magnetisms. This family provides a promising material platform for promoting the further explorations on the exotic magnetic topological phases and the related topological quantum transport studies.

Results

The structure of $RETi_3Bi_4$ is displayed in Fig. 1(a), and Fig. 1(b) shows the clean kagome layer of Ti with distorted slightly from the identical positions, less than 0.1 \AA for $EuTi_3Bi_4$ for example. $RETi_3Bi_4$ holds larger prototype structures which have four kagome layers per unit cell, compared with other kagome materials like RT_6X_6 ($R = \text{rare earth}; T = V, Cr, Mn, Fe, Co; X = Ge, Sn$) and AV_3Sb_5 ($A = K, Rb, Cs$), and forms a orthogonal lattice structure with $Fmmm$ space group (No. 69)³⁸⁻⁴⁰. The interlayer interactions between the adjacent RE/Bi layers are weak due to the limited spatial density of the $RE-RE$ zig-zag-chain-shaped chemical bonds shown in Fig. 1(c). This

kind of weak bond interactions can also be found in KV_3Sb_5 family of materials. Thus, similar to the cleavable lattice layers in KV_3Sb_5 family, it is expected that $EuTi_3Bi_4$ can also be exfoliated by knives or tapes, and thin flakes of $EuTi_3Bi_4$ can be obtained to make device fabricating available. The crystals of $EuTi_3Bi_4$, $GdTi_3Bi_4$, and $SmTi_3Bi_4$ are grown by flux method as seen in Fig. 1(f). Fig. 1(d) shows the single crystal X-ray diffraction (XRD) pattern of the hexagonal surface of $RETi_3Bi_4$, indicating the high quality of $RETi_3Bi_4$ with $c \approx 25.46 \text{ \AA}$, 24.81 \AA and 24.89 \AA for Eu, Gd and Sm. Although these three samples are adjoined each other on periodic table, the length of c axis of $EuTi_3Bi_4$ are significantly larger than other two samples, which might be caused by the abnormal lanthanide contraction of Eu. Fig. 1(e) displays the energy dispersive spectra (EDS) for samples with different rare earth elements as Eu, Gd and Sm. The ratio of RE: Ti: Bi is nearly 1:3:4, indicating a stoichiometric atomic ratio.

Due to the weak interlayer interactions between two adjacent RE/Bi layers, $RETi_3Bi_4$ family is expected to be cleavable by knives or tapes. To verify it, by repeatedly stacking on the crystal surface with two pieces of tape (Nitto, BT-150E-KL), large number of shiny pieces are symmetrically distributed on both sides of the tapes (Fig. 2(a)), indicating the sufficient exfoliation of $RETi_3Bi_4$. By pressing the tape onto silicon wafers with 300 nm SiO_2 on top, one can further obtain $RETi_3Bi_4$ nano-flakes with dozens of micrometers on lateral sizes as displayed in Fig.2(b)-(d). The flakes all show blue or cyan color, indicating the thin thickness as low as nanometers. By scanning the thickness of these flakes through an atomic force microscope (AFM), one can see that the thickness are varies from 5 nm to dozens of nanometers, as displayed by the red line-scanning curves overlay on the respective optical images in Fig. 2(b)-(d). These results confirm that $RETi_3Bi_4$ family is cleavable and suggest the feasibility for mesoscopic device fabrications.

We then study the magnetic properties of $RETi_3Bi_4$ family utilizing a vibrating sample magnetometer (VSM). The results are summarized in Fig. 3. Fig. 3(a)-(c) display the magnetization versus external magnetic field ($M-H$) of $EuTi_3Bi_4$ ($H//c$), $GdTi_3Bi_4$ ($H//c$), and $SmTi_3Bi_4$ ($H//ab$ plane) respectively under various temperatures from 2 K to 50 K. In Fig. 3(a), one can clearly see a typical soft out-of-plane ferromagnetic type $M-H$ curves of $EuTi_3Bi_4$. A hysteresis loop with coercive field 130 Oe is received under the temperature of 2 K, and the magnetic moments are saturated

when increasing the magnetic field up to 0.4 T. The saturation magnetization (M_s) of EuTi_3Bi_4 is $\sim 5.3 \mu_B/\text{f. u.}$ taking into the six 4f electrons of Eu^{3+} , and the results are consistent with a ferromagnetic order of EuTi_3Bi_4 . The M_s provided by Eu about $5\mu_B$ are also be observed in recent research of the EuV_3Sb_4 , the variation of RETi_3Bi_4 ⁴¹. The inset displays magnetic moments saturates under lower fields when applying fields along c axis ($H//c$) comparing with the case for $H//ab$ plane, pointing out that for EuTi_3Bi_4 , the easy axis are along c axis. Fig. 3(b) shows the magnetization versus temperature under a fixed magnetic field of 100 Oe. By sweeping the temperature through a zero-field-cooling (ZFC) and a field-cooling (FC) processes, one can see that the magnetization rises quickly when the temperatures are lower than 15 K, and a typical divarication between ZFC and FC curves of ferromagnetic order can be identified. By taking the 1st derivative of the FC curve, Curie temperature (T_C) of 11 K is obtained by extracting the temperature value at the extremum of the derivative curve. For the M - H curves of GdTi_3Bi_4 in Fig. 3(c), one can identify that GdTi_3Bi_4 holds an out-of-plane AFM order with zero net magnetization under zero magnetic field. By applying magnetic fields, two steps of spin flop transitions with the critical fields of $H_{c1} = 1.6$ T and $H_{c2} = 3.3$ T can be observed. This kind of multiple spin flop transitions are also previous reported in several AFM magnets^{27,42-44}. Saturation magnetization M_s of $\sim 6.7 \mu_B/\text{f. u.}$, which is also close to the ideal $7 \mu_B$ from Gd^{3+} ions, is received when the field is larger than 6 T in GdTi_3Bi_4 . The inset of Fig. 3(c) displays the magnetic moments saturates under lower fields when applying fields along c axis ($H//c$) and for $H//ab$ plane, indicating that for GdTi_3Bi_4 , the easy axis are along c axis, same as in EuTi_3Bi_4 . The FC and ZFC curves of GdTi_3Bi_4 in Fig. 3(d) coincide exactly under all temperatures, and a representative kink feature can be identified as marked by the arrow, which indicates the Néel temperature of 14.5 K. Contrary to the out-of-plane magnetic order in EuTi_3Bi_4 and GdTi_3Bi_4 , SmTi_3Bi_4 shows rather small in-plane ferromagnetism under low temperatures and high magnetic field in Fig. 3(e). The inset displays the magnetic moments saturates under lower fields when applying fields along c axis ($H//c$) comparing with the case for $H//ab$ plane, and the orbital magnetic moment may cause the diamagnetic contribution of the negative signal when $H//ab$. The magnetization versus temperature of SmTi_3Bi_4 under a fixed magnetic field of 100 Oe are displayed in Fig. 3(f). The ZFC and FC curves show a ferromagnetic order, and the 1st derivative of the FC curve, Curie temperature (T_C) of 23.3 K is also obtained.

One may notice that the magnetism in RETi_3Bi_4 family is simple comparing with those magnetic kagome materials with complex magnetic orders, and the M_s value of the samples with spontaneous magnetization are relatively large for EuTi_3Bi_4 and GdTi_3Bi_4 . We attribute these two points to the reason that only rare earth elements in RETi_3Bi_4 family contribute the magnetic order. The magnetic moments containing in each rare earth atom or kation are relatively larger than the ones in transition metal elements. In addition, the factor that Ti kagome lattices in RETi_3Bi_4 do not contribute the magnetic order also benefits the formation of a simple magnetic order with large M_s . The reason is that the moments provided by the kagome lattices formed by magnetic elements may align oppositely to the ones provided by rare earth elements¹⁹, forming frustrated magnetism¹¹, or forming complex spiral magnetisms⁴⁵.

The band structures of RETi_3Bi_4 family are also investigated in this work. Here, we take EuTi_3Bi_4 as the representative to elucidate the exotic electronic properties of these materials with kagome sublattices. Fig. 4(a) presents the first Brillouin zone, the high-symmetry k points, and the corresponding two-dimensional projected surface of EuTi_3Bi_4 primitive cell. The calculated results are in great agreement with the experimental results when $U = 6$ eV by comparing. Fig. 4(b) illustrates the band structure of EuTi_3Bi_4 with SOC in FM state. Obviously, we can observe the bands with van Hove singularity (vHs)-like at point Y known as saddle-type bands. For the sake of greater clarity, we calculate the bands contributed by $3d$ orbitals of Ti atoms forming the kagome sublattice along a high-symmetric k path as close to the hexagon Brillouin zone (BZ) as possible, as depicted in Fig. 4(c). The typical band characteristics caused by the kagome structure are roughly plotted with blue lines in Fig. 4(c). Around the point C_0 , we discover the distinct bands with Dirac cone-like above the Fermi level about 0.1 eV and the flat bands are located above them about 1.5 eV. These calculation results are typical characteristic of bands for the materials with kagome sublattice.

For further exploring the surface electronic properties of EuTi_3Bi_4 , we calculate the surface states from bulk part and the corresponding Fermi surface on 2D projected surface of EuTi_3Bi_4 as illustrated in Fig. 4(d) and (e), respectively. A similar kagome bands can also be discovered in Fig. 4(d). In Fig. 4(e), we can observe six petal-like

Fermi surface patterns. These results are agreed well with the experimental measurements as follows. However, due to the predicted Dirac cone-like bands are above the Fermi level, it is difficult to be observed in experimental measurements.

We then investigate the band structure of RETi_3Bi_4 via ARPES measurement. By mapping out the ARPES dispersions detected under various photon energies, the out-of-plane (k_x - k_z plane) constant energy contours (CECs) near E_F can be obtained as seen in Fig. 5(a). The CECs along k_z direction show no clear cyclical change along with BZ, indicating the quasi-2D property of the dispersion in RETi_3Bi_4 . In Fig. 5(b), the Fermi surface structures of EuTi_3Bi_4 , GdTi_3Bi_4 , and SmTi_3Bi_4 are demonstrated. One can clearly see similar hexagonal contours in all three materials. For EuTi_3Bi_4 , one can see the strong signals at the K points of the first BZ which correspond to the six petal-like Fermi surface patterns obtained by calculations in Fig. 4(e). The ring-shaped pocket surrounding Γ point and the finite density of states at Γ point can also be identified in the second BZ. These results are consistent with the calculation demonstrated above. The finite density of states at Γ point in EuTi_3Bi_4 evolves to an annular-shaped pocket in the case of GdTi_3Bi_4 (red dotted circle) and SmTi_3Bi_4 , indicating the Fermi energy of GdTi_3Bi_4 , and SmTi_3Bi_4 is higher than EuTi_3Bi_4 since an electron pocket is expected at Γ point according to the calculation. Fig. 5(c)-(e) displays the detected band dispersions along Γ - C_0 direction of EuTi_3Bi_4 , GdTi_3Bi_4 , and SmTi_3Bi_4 respectively. By overlay the calculation on the ARPES results in the Eu case in Fig. 5(c), we can find that the ARPES results are quantitatively match with the calculated dispersions with a large V-shaped dispersion crossing C_0 - Γ - C_0 , indicating the veracity of the band calculations in Fig. 4. Additionally, the flat bands caused by Eu are also observed between -1.5 and -2.0 eV in Fig. 5(c). In Fig. 5(d) and (e), band dispersions of GdTi_3Bi_4 and SmTi_3Bi_4 are similar to those in EuTi_3Bi_4 . The difference is that the Fermi energy is ~ 0.3 eV higher than EuTi_3Bi_4 , and the conduction band minimum of a branch of conduction band at Γ point is lower than E_F in GdTi_3Bi_4 , becoming detectable by our ARPES measurement as marked by the red dotted curves in Fig.5(d).

Summary

In conclusion, we systematically investigate a new family RETi_3Bi_4 (RE = Eu, Gd and Sm) with weak interlayer interactions and clean kagome layers via magnetic

measurement, ARPES measurement and first-principles calculation. The weak interlayer interactions between adjacent RE/Bi caused by the limited spatial density of the RE-RE zig-zag chain shaped chemical bonds make it easy to do mechanical exfoliation until nanometer scale. The rare earth elements solely provide the magnetic moments in RETi_3Bi_4 , and magnetisms of FM, AFM, and PM are formed for RE = Eu, Gd, and Sm respectively. The magnetic orders are simple and the saturation magnetization are relatively large in EuTi_3Bi_4 and GdTi_3Bi_4 comparing with the previous studied transition metal based kagome lattices. The first-principle calculations and ARPES are consistent with each other. We provide insights into the electronic structure of RETi_3Bi_4 family, suggesting an ideal platform to investigate the exotic magnetic topological phases and the related topological quantum transport studies. We believe that this new Kagome magnets family is worthy of further studies on kagome physics and offer a wide range of potential applications in the future.

Add note: We noticed a recent study on the same family of material RETi_3Bi_4 (RE = Yb, Pr, and Nd)⁴⁶, in which the tunable magnetism and electron correlation are studied. These two studies complement each other and show more plentiful properties in this family of material.

Methods

Crystal Growth. The flux method is utilized to synthesize the high-quality single crystals. The starting elements of Eu (Gd, Sm): Ti: Bi in the molar ratio of 1.2: 1: 20 are mixed in an alumina crucible and sealed in a quartz ampule. The ampule is placed in a furnace and heated to 1000 °C at a rate of 1 °C/min. After maintaining it at 1000 °C for 16 h, the ampule is slowly cooled down to 520 °C in 2000 min. The hexagonal shaped single crystals are obtained after centrifuging in order to remove the excess flux.

Magnetic Measurements. Magnetic properties are measured with a Physical Properties Measurement System (Quantum Design) in the temperature range $2 \text{ K} \leq T$

≤ 300 K with magnetic field up to 9 T. Standard copper holders and quartz holders are used during the measurements when $H//c$ and $H//ab$ respectively.

ARPES. ARPES experiments are performed at the BL03U and the BL09U beamlines at the Shanghai Synchrotron Radiation Facility. Data is collected with photon energies ranging from 48 to 120 eV with linear horizontal polarization. The samples are cleaved and measured in an ultrahigh-vacuum chamber at a pressure below 10^{-10} Torr.

Band Structures Calculations. The band structures calculations of EuTi_3Bi_4 are performed by the Vienna ab initio Simulation package (VASP) with the projector augmented-wave (PAW) formalism based on the density functional theory (DFT)^{47,48}. The Perdew-Burke-Ernzerhof (PBE) exchange-correlation functional with the generalized gradient approximation corrected for on-site Coulombic interactions (GGA + U) method is adopted^{49,50}. The parameter U is selected to be 6 eV to treat the effect of Coulomb correction from the localized $4f$ orbitals of Eu atoms. The cutoff energy for the plane-wave basis is set at 520 eV and the Brillouin zone (BZ) integral is sampled by $7 \times 7 \times 7$ Γ -centered k mesh. The local magnetic moments on Eu atoms for ferromagnetic state (FM) are along the z axis. Spin-orbit coupling (SOC) is taken into account in all calculations. The tight-binding model of EuTi_3Bi_4 is constructed by the Wannier90 with Eu $4f$ orbitals, Ti $3d$ orbitals, and Bi $6p$ orbitals based on the maximally-localized Wannier functions (MLWF)⁵¹. The surface states and the corresponding Fermi surface are calculated by using the WannierTools software package⁵².

Acknowledgments

The authors gratefully acknowledge the financial support of the National Key Research and Development Program of China (Grant No. 2022YFA1402404); the National Natural Science Foundation of China (Grant Nos. 92161201, T2221003, 12104221, 12104220, 12274208, 12025404, 12004174, 91961101, 61822403, 11874203, 12104220); the Fundamental Research Funds for the Central Universities

(Grant No. 020414380192). Part of this research used Beamline 03U of the Shanghai Synchrotron Radiation Facility, which is supported by ME2 project under Contract No.11227902 from National Natural Science Foundation of China. The authors also thank Professor Peng Zhang from Nanjing University for discussions.

Data availability

The datasets that support the findings of this study are available from the corresponding author upon reasonable request.

References

- 1 Tian-Heng Han, J. S. H., Shaoyan Chu, Daniel G. Nocera, Jose A. Rodriguez-Rivera, Collin Broholm & Young S. Lee. Fractionalized excitations in the spin-liquid state of a kagome-lattice antiferromagnet. *Nature* **492**, 406-410 (2012).
- 2 Stefan Depenbrock, I. P. M., and Ulrich Schollwock. Nature of the spin-liquid ground state of the $S=1/2$ Heisenberg model on the kagome lattice. *Phys. Rev. Lett.* **109**, 067201 (2012).
- 3 Sachdev, S. Kagome- and triangular-lattice Heisenberg antiferromagnets: Ordering from quantum fluctuations and quantum-disordered ground states with unconfined bosonic spinons. *Phys. Rev. B* **45**, 12377-12396 (1992).
- 4 D. F. Liu, A. J. Liang, E. K. Liu, Q.N.Xu, Y. W. Li, C. Chen, D. Pei, W. J. Shi, S.K.Mo, P. Dudin, T. Kim, C. Cacho, G. Li, Y. Sun, L. X. Yang, Z. K. Liu, S. S. P. Parkin, C. Felser & Chen, Y. L. Magnetic Weyl semimetal phase in a Kagomé crystal. *Science* **365**, 1282–1285 (2019).
- 5 Yin, J.-X., Lian, B. & Hasan, M. Z. Topological kagome magnets and superconductors. *Nature* **612**, 647-657 (2022).
- 6 Kenya Ohgushi, S. M., and Naoto Nagaosa. Spin anisotropy and quantum Hall effect in the kagome' lattice: Chiral spin state based on a ferromagnet. *Phys. Rev. B* **62**, R6065-R6068 (2000).
- 7 I.I. Mazin, H. O. J., Frank Lechermann, Hunpyo Lee, Mario Fink, Ronny Thomale & Roser Valentí. Theoretical prediction of a strongly correlated Dirac metal. *Nat. Commun.* **5**, 4261 (2014).
- 8 Xu, G., Lian, B. & Zhang, S. C. Intrinsic Quantum Anomalous Hall Effect in the Kagome Lattice Cs₂LiMn₃F₁₂. *Phys. Rev. Lett.* **115**, 186802 (2015).
- 9 Kang, M., Ye, L., Fang, S., You, J. S., Levitan, A., Han, M., Facio, J. I., Jozwiak, C., Bostwick, A., Rotenberg, E., Chan, M. K., McDonald, R. D., Graf, D., Kaznatcheev, K., Vescovo, E., Bell, D. C., Kaxiras, E., van den Brink, J., Richter, M., Prasad Ghimire, M., Checkelsky, J. G. & Comin, R. Dirac fermions and flat bands in the ideal kagome metal FeSn. *Nat. Mater.* **19**, 163-169 (2020).

- 10 Kang, M., Fang, S., Ye, L., Po, H. C., Denlinger, J., Jozwiak, C., Bostwick, A., Rotenberg, E., Kaxiras, E., Checkelsky, J. G. & Comin, R. Topological flat bands in frustrated kagome lattice CoSn. *Nat. Commun.* **11**, 4004 (2020).
- 11 Nakatsuji, S., Kiyohara, N. & Higo, T. Large anomalous Hall effect in a non-collinear antiferromagnet at room temperature. *Nature* **527**, 212-215 (2015).
- 12 Wang, Q., Xu, Y., Lou, R., Liu, Z., Li, M., Huang, Y., Shen, D., Weng, H., Wang, S. & Lei, H. Large intrinsic anomalous Hall effect in half-metallic ferromagnet Co(3)Sn(2)S(2) with magnetic Weyl fermions. *Nat. Commun.* **9**, 3681 (2018).
- 13 Liu, E., Sun, Y., Kumar, N., Muchler, L., Sun, A., Jiao, L., Yang, S. Y., Liu, D., Liang, A., Xu, Q., Kroder, J., Suss, V., Borrmann, H., Shekhar, C., Wang, Z., Xi, C., Wang, W., Schnelle, W., Wirth, S., Chen, Y., Goennenwein, S. T. B. & Felser, C. Giant anomalous Hall effect in a ferromagnetic Kagome-lattice semimetal. *Nat. Phys.* **14**, 1125-1131 (2018).
- 14 Kuroda, K., Tomita, T., Suzuki, M. T., Bareille, C., Nugroho, A. A., Goswami, P., Ochi, M., Ikhlas, M., Nakayama, M., Akebi, S., Noguchi, R., Ishii, R., Inami, N., Ono, K., Kumigashira, H., Varykhalov, A., Muro, T., Koretsune, T., Arita, R., Shin, S., Kondo, T. & Nakatsuji, S. Evidence for magnetic Weyl fermions in a correlated metal. *Nat. Mater.* **16**, 1090-1095 (2017).
- 15 Ajaya K. Nayak, J. E. F., Yan Sun, Binghai Yan, Julie Karel, Alexander C. Komarek, Chandra Shekhar, Nitesh Kumar, Walter Schnelle, Jürgen Kübler, Claudia Felser, Stuart S. P. Parkin. Large anomalous Hall effect driven by a nonvanishing Berry curvature in the noncollinear antiferromagnet Mn₃Ge. *Sci. Adv.* **2**, e1501870 (2016).
- 16 Zhonghao, L., Man, L., Qi, W., Guangwei, W., Chenhaoping, W., Kun, J., Xiangle, L., Shichao, Y., Yaobo, H., Dawei, S., Jia-Xin, Y., Ziqiang, W., Zhiping, Y., Hechang, L. & Shancai, W. Orbital-selective Dirac fermions and extremely flat bands in frustrated kagome-lattice metal CoSn. *Nat. Commun.* **11**, 4002 (2020).
- 17 Ye, L., Chan, M. K., McDonald, R. D., Graf, D., Kang, M., Liu, J., Suzuki, T., Comin, R., Fu, L. & Checkelsky, J. G. de Haas-van Alphen effect of correlated Dirac states in kagome metal Fe(3)Sn(2). *Nat. Commun.* **10**, 4870 (2019).
- 18 Ye, L., Kang, M., Liu, J., von Cube, F., Wicker, C. R., Suzuki, T., Jozwiak, C., Bostwick, A., Rotenberg, E., Bell, D. C., Fu, L., Comin, R. & Checkelsky, J. G. Massive Dirac fermions in a ferromagnetic kagome metal. *Nature* **555**, 638-642 (2018).
- 19 Yin, J. X., Ma, W., Cochran, T. A., Xu, X., Zhang, S. S., Tien, H. J., Shumiya, N., Cheng, G., Jiang, K., Lian, B., Song, Z., Chang, G., Belopolski, I., Multer, D., Litskevich, M., Cheng, Z. J., Yang, X. P., Swidler, B., Zhou, H., Lin, H., Neupert, T., Wang, Z., Yao, N., Chang, T. R., Jia, S. & Zahid Hasan, M. Quantum-limit Chern topological magnetism in TbMn(6)Sn(6). *Nature* **583**, 533-536 (2020).
- 20 Nirmal J Ghimire, Rebecca L. Dally, L. Poudel, D. C. Jones, D. Michel, N. Thapa Magar, M. Bleuel, Michael A. McGuire, J. S. Jiang, J. F. Mitchell,

- Jeffrey W. Lynn & Mazin, I. I. Competing magnetic phases and fluctuation-driven scalar spin chirality in the kagome metal YMn₆Sn₆. *Sci. Adv.* **6**, eabe2680 (2020).
- 21 Li, M., Wang, Q., Wang, G., Yuan, Z., Song, W., Lou, R., Liu, Z., Huang, Y., Liu, Z., Lei, H., Yin, Z. & Wang, S. Dirac cone, flat band and saddle point in kagome magnet YMn(6)Sn(6). *Nat. Commun.* **12**, 3129 (2021).
- 22 Liu, Z., Zhao, N., Li, M., Yin, Q., Wang, Q., Liu, Z., Shen, D., Huang, Y., Lei, H., Liu, K. & Wang, S. Electronic correlation effects in the kagome magnet GdMn₆Sn₆. *Phys. Rev. B* **104**, 115122 (2021).
- 23 Dong Chen, Congcong Le, Chenguang Fu, Haicheng Lin, Walter Schnelle, Yan Sun & Felser, C. Large anomalous Hall effect in the kagome ferromagnet LiMn₆Sn₆. *Phys. Rev. B* **103**, 144410 (2021).
- 24 Ma, W., Xu, X., Yin, J.-X., Yang, H., Zhou, H., Cheng, Z.-J., Huang, Y., Qu, Z., Wang, F., Hasan, M. Z. & Jia, S. Rare Earth Engineering in RMn₆Sn₆(R=Gd–Tm, Lu) Topological Kagome Magnets. *Phys. Rev. Lett.* **126**, 246602 (2021).
- 25 G. Venturini, B. C. E. I., B. Malaman,. Magnetic properties of RMn₆Sn₆ (R = Sc, Y, Gd–Tm, Lu) compounds with HfFe₆Ge₆ type structure. *J. Magn. Magn. Mater.* **94**, 35-42 (1991).
- 26 Peng, S., Han, Y., Pokharel, G., Shen, J., Li, Z., Hashimoto, M., Lu, D., Ortiz, B. R., Luo, Y., Li, H., Guo, M., Wang, B., Cui, S., Sun, Z., Qiao, Z., Wilson, S. D. & He, J. Realizing Kagome Band Structure in Two-Dimensional Kagome Surface States of RV₆Sn₆ (R=Gd, Ho). *Phys. Rev. Lett.* **127**, 266401 (2021).
- 27 Ortiz, B. R., Gomes, L. C., Morey, J. R., Winiarski, M., Bordelon, M., Mangum, J. S., Oswald, I. W. H., Rodriguez-Rivera, J. A., Neilson, J. R., Wilson, S. D., Ertekin, E., McQueen, T. M. & Toberer, E. S. New kagome prototype materials: discovery of KV₃Sb₅, RbV₃Sb₅, and CsV₃Sb₅. *Phys. Rev. Mater.* **3**, 094407 (2019).
- 28 Song, Y., Ying, T., Chen, X., Han, X., Wu, X., Schnyder, A. P., Huang, Y., Guo, J.-g. & Chen, X. Competition of Superconductivity and Charge Density Wave in Selective Oxidized CsV₃Sb₅ Thin Flakes. *Phys. Rev. Lett.* **127**, 237001 (2021).
- 29 Song, B., Ying, T., Wu, X., Xia, W., Yin, Q., Zhang, Q., Song, Y., Yang, X., Guo, J., Gu, L., Chen, X., Hu, J., Schnyder, A. P., Lei, H., Guo, Y. & Li, S. Anomalous enhancement of charge density wave in kagome superconductor CsV₃Sb₅ approaching the 2D limit. *Nat. Commun.* **14**, 2492 (2023).
- 30 Zheng, G., Tan, C., Chen, Z., Wang, M., Zhu, X., Albarakati, S., Algarni, M., Partridge, J., Farrar, L., Zhou, J., Ning, W., Tian, M., Fuhrer, M. S. & Wang, L. Electrically controlled superconductor-to-failed insulator transition and giant anomalous Hall effect in kagome metal CsV₃Sb₅ nanoflakes. *Nat. Commun.* **14**, 678 (2023).
- 31 Li, H., Zhang, T. T., Yilmaz, T., Pai, Y. Y., Marvinney, C. E., Said, A., Yin, Q. W., Gong, C. S., Tu, Z. J., Vescovo, E., Nelson, C. S., Moore, R. G., Murakami, S., Lei, H. C., Lee, H. N., Lawrie, B. J. & Miao, H. Observation of

- Unconventional Charge Density Wave without Acoustic Phonon Anomaly in Kagome Superconductors AV₃Sb₅(A=Rb, Cs). *Phys. Rev. X* **11**, 031050 (2021).
- 32 Chen, H., Yang, H., Hu, B., Zhao, Z., Yuan, J., Xing, Y., Qian, G., Huang, Z., Li, G., Ye, Y., Ma, S., Ni, S., Zhang, H., Yin, Q., Gong, C., Tu, Z., Lei, H., Tan, H., Zhou, S., Shen, C., Dong, X., Yan, B., Wang, Z. & Gao, H. J. Roton pair density wave in a strong-coupling kagome superconductor. *Nature* **599**, 222-228 (2021).
- 33 Liang, Z., Hou, X., Zhang, F., Ma, W., Wu, P., Zhang, Z., Yu, F., Ying, J. J., Jiang, K., Shan, L., Wang, Z. & Chen, X. H. Three-Dimensional Charge Density Wave and Surface-Dependent Vortex-Core States in a Kagome Superconductor CsV₃Sb₅. *Phys. Rev. X* **11**, 031026 (2021).
- 34 Jiang, Y. X., Yin, J. X., Denner, M. M., Shumiya, N., Ortiz, B. R., Xu, G., Guguchia, Z., He, J., Hossain, M. S., Liu, X., Ruff, J., Kautzsch, L., Zhang, S. S., Chang, G., Belopolski, I., Zhang, Q., Cochran, T. A., Multer, D., Litskevich, M., Cheng, Z. J., Yang, X. P., Wang, Z., Thomale, R., Neupert, T., Wilson, S. D. & Hasan, M. Z. Unconventional chiral charge order in kagome superconductor KV(3)Sb(5). *Nat. Mater.* **20**, 1353-1357 (2021).
- 35 Luo, H., Gao, Q., Liu, H., Gu, Y., Wu, D., Yi, C., Jia, J., Wu, S., Luo, X., Xu, Y., Zhao, L., Wang, Q., Mao, H., Liu, G., Zhu, Z., Shi, Y., Jiang, K., Hu, J., Xu, Z. & Zhou, X. J. Electronic nature of charge density wave and electron-phonon coupling in kagome superconductor KV(3)Sb(5). *Nat. Commun.* **13**, 273 (2022).
- 36 Cho, S., Ma, H., Xia, W., Yang, Y., Liu, Z., Huang, Z., Jiang, Z., Lu, X., Liu, J., Liu, Z., Li, J., Wang, J., Liu, Y., Jia, J., Guo, Y., Liu, J. & Shen, D. Emergence of New van Hove Singularities in the Charge Density Wave State of a Topological Kagome Metal RbV₃Sb₅. *Phys. Rev. Lett.* **127**, 236401 (2021).
- 37 Chen, K. Y., Wang, N. N., Yin, Q. W., Gu, Y. H., Jiang, K., Tu, Z. J., Gong, C. S., Uwatoko, Y., Sun, J. P., Lei, H. C., Hu, J. P. & Cheng, J. G. Double Superconducting Dome and Triple Enhancement of T_c in the Kagome Superconductor CsV₃Sb₅ under High Pressure. *Phys. Rev. Lett.* **126**, 247001 (2021).
- 38 Motoyama, G., Sezaki, M., Gouchi, J., Miyoshi, K., Nishigori, S., Mutou, T., Fujiwara, K. & Uwatoko, Y. Magnetic properties of new antiferromagnetic heavy-fermion compounds, Ce₃TiBi₅ and CeTi₃Bi₄. *Phys. Rev., B Condens. Matter* **536**, 142-144 (2018).
- 39 Ovchinnikov, A. & Bobev, S. Synthesis, Crystal and Electronic Structure of the Titanium Bismuthides Sr₅Ti₁₂Bi_{19+x}, Ba₅Ti₁₂Bi_{19+x}, and Sr_{5-δ}Eu_δTi₁₂Bi_{19+x}(x ≈ 0.5 - 1.0; δ ≈ 2.4, 4.0). *Eur. J. Inorg. Chem.* **2018**, 1266-1274 (2018).
- 40 Ovchinnikov, A. & Bobev, S. Bismuth as a Reactive Solvent in the Synthesis of Multicomponent Transition-Metal-Bearing Bismuthides. *Inorg. Chem.* **59**, 3459-3470 (2019).
- 41 Brenden R. Ortiz, G. P., Malia Gundayao, Hong Li, Farnaz Kaboudvand, Linus

- Kautzsch, Suchismita Sarker, Jacob P. C. Ruff, Tom Hogan, Steven J. Gomez Alvarado, Paul M. Sarte, Guang Wu, Tara Braden, Ram Seshadri, Eric S. Toberer, Ilija Zeljkovic, and Stephen D. Wilson. YbV₃Sb₄ and EuV₃Sb₄, vanadium-based kagome metals with Yb²⁺ and Eu²⁺ zig-zag chains. *arXiv: 2302.12354* (2023).
- 42 Thompson, C. M., Tan, X., Kovnir, K., Garlea, V. O., Gippius, A. A., Yaroslavtsev, A. A., Menushenkov, A. P., Chernikov, R. V., Büttgen, N., Krätschmer, W., Zubavichus, Y. V. & Shatruk, M. Synthesis, Structures, and Magnetic Properties of Rare-Earth Cobalt Arsenides, RCo₂As₂ (R = La, Ce, Pr, Nd). *Chem. Mater.* **26**, 3825-3837 (2014).
- 43 Yang, S., Xu, X., Zhu, Y., Niu, R., Xu, C., Peng, Y., Cheng, X., Jia, X., Huang, Y., Xu, X., Lu, J. & Ye, Y. Odd-Even Layer-Number Effect and Layer-Dependent Magnetic Phase Diagrams in MnBi₂Te₄. *Phys. Rev. X* **11** (2021).
- 44 Tan, X., Garlea, V. O., Kovnir, K., Thompson, C. M., Xu, T., Cao, H., Chai, P., Tener, Z. P., Yan, S., Xiong, P. & Shatruk, M. Complex magnetic phase diagram with multistep spin-flop transitions in La_{0.25}Pr_{0.75}Co₂P₂. *Phys. Rev. B* **95**, 024428 (2017).
- 45 P. Schobinger-Papamantellos, F.B. Altorfer, J.H.V.J. Brabers, F.R. de Boer & Buschow, K. H. J. Magnetic properties of DyMn₆Ge₆ studied by neutron diffraction and magnetic measurements. *J. Alloys Compd.* **203**, 243-250 (1994).
- 46 Long Chen, Y. Z., He Zhang, Xuecong Ji, Ke Liao, Yu Ji, Ying Li, Zhongnan Guo, Xi Shen, Richeng Yu, Xiaohui Yu, Hongming Weng, Gang Wang. Tunable magnetism and electron correlation in Titanium-based Kagome metals RETi₃Bi₄ (RE = Yb, Pr, and Nd) by rare-earth engineering. *arXiv: 2307.02942* (2023).
- 47 G. Kresse, J. F. I. Efficient iterative schemes for ab initio total-energy calculations using a plane-wave basis set. *Phys. Rev. B* **54**, 11169-11111 11186 (1996).
- 48 G. Kresse, D. J. From ultrasoft pseudopotentials to the projector augmented-wave method. *Phys. Rev. B* **59**, 1758-1775 (1999).
- 49 John P. Perdew, K. B., * Matthias Ernzerhof. Generalized Gradient Approximation Made Simple. *Phys. Rev. Lett.* **77**, 3865-3868 (1996).
- 50 Heather J. Kulik, M. C., Damian A. Scherlis,* and Nicola Marzari. Density Functional Theory in Transition-Metal Chemistry: A Self-Consistent HubbardU Approach. *Phys. Rev. Lett.* **97**, 103001 (2006).
- 51 Mostofi, A. A., Yates, J. R., Pizzi, G., Lee, Y.-S., Souza, I., Vanderbilt, D. & Marzari, N. An updated version of wannier90: A tool for obtaining maximally-localised Wannier functions. *Comput. Phys. Commun.* **185**, 2309-2310 (2014).
- 52 Wu, Q., Zhang, S., Song, H.-F., Troyer, M. & Soluyanov, A. A. WannierTools: An open-source software package for novel topological materials. *Comput. Phys. Commun.* **224**, 405-416 (2018).

Competing interests

The authors declare no competing financial interests.

Figures

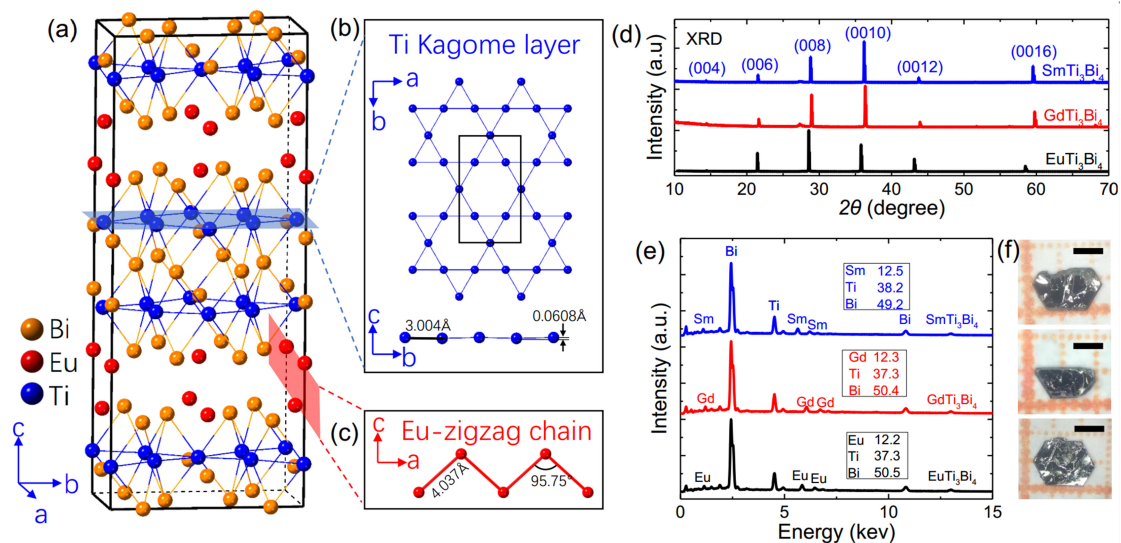


Fig. 1. Crystal structures and characterizations. (a) Crystal structure diagrams of EuTi_3Bi_4 . (b) The diagram of Ti kagome layer with slightly distortion along c axis. (c) The diagram of zigzag chain formed by rare earth elements (d) Single crystal XRD pattern for RETi_3Bi_4 samples. (e) EDS results of RETi_3Bi_4 . (f) Optical photographs of as-grown RETi_3Bi_4 crystals. Scale bar: 1 mm.

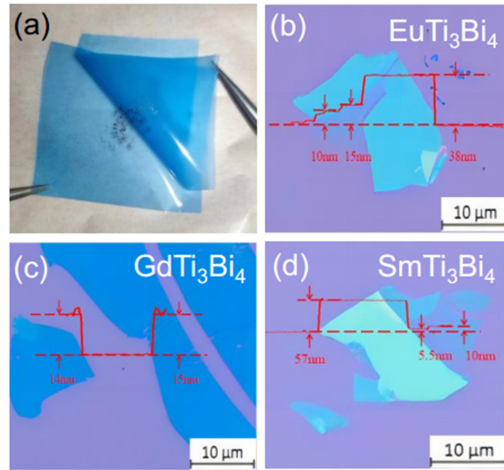


Fig. 2. Mechanical exfoliation of RETi_3Bi_4 . (a) The demonstration of mechanical exfoliation of RETi_3Bi_4 by tapes. (b-d) Optical images and the corresponding AFM line-scanning profiles of the few-layer flakes of EuTi_3Bi_4 , GdTi_3Bi_4 , and SmTi_3Bi_4 respectively.

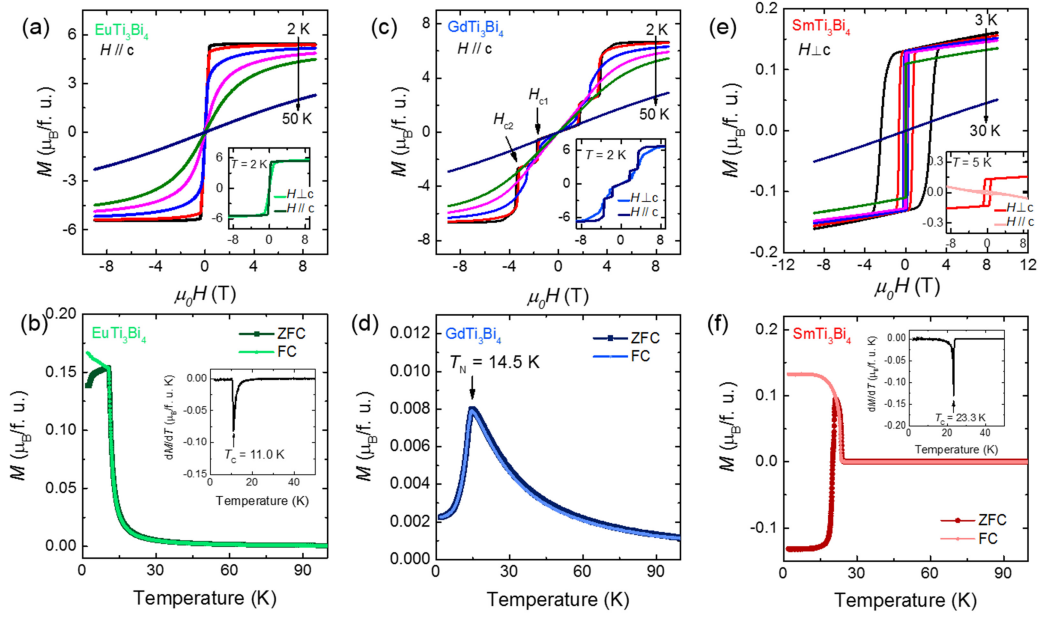


Fig. 3. Magnetic measurements. (a) Magnetization versus magnetic field for EuTi_3Bi_4 at 2 K, 5 K, 10 K, 15 K, 20 K and 50 K, $H//c$. The inset displays M - H curves along c axis ($H//c$) and $H//ab$ plane of EuTi_3Bi_4 at 2 K. (b) FC-ZFC curves of EuTi_3Bi_4 under an external magnetic field of 100 Oe ($H//c$). The inset displays the 1st derivative of FC curves. (c) The same as (a) but for GdTi_3Bi_4 . (d) The same as (b) but for GdTi_3Bi_4 . (e) M - H curves for SmTi_3Bi_4 at 3 K, 5 K, 10 K, 15 K, 20 K and 30 K, $H//ab$. The inset displays the M - H curves along c axis ($H//c$) and $H//ab$ plane of SmTi_3Bi_4 at 5 K. (f) FC-ZFC curves of SmTi_3Bi_4 under an external magnetic field of 100 Oe ($H//ab$). The inset displays the 1st derivative of FC curves.

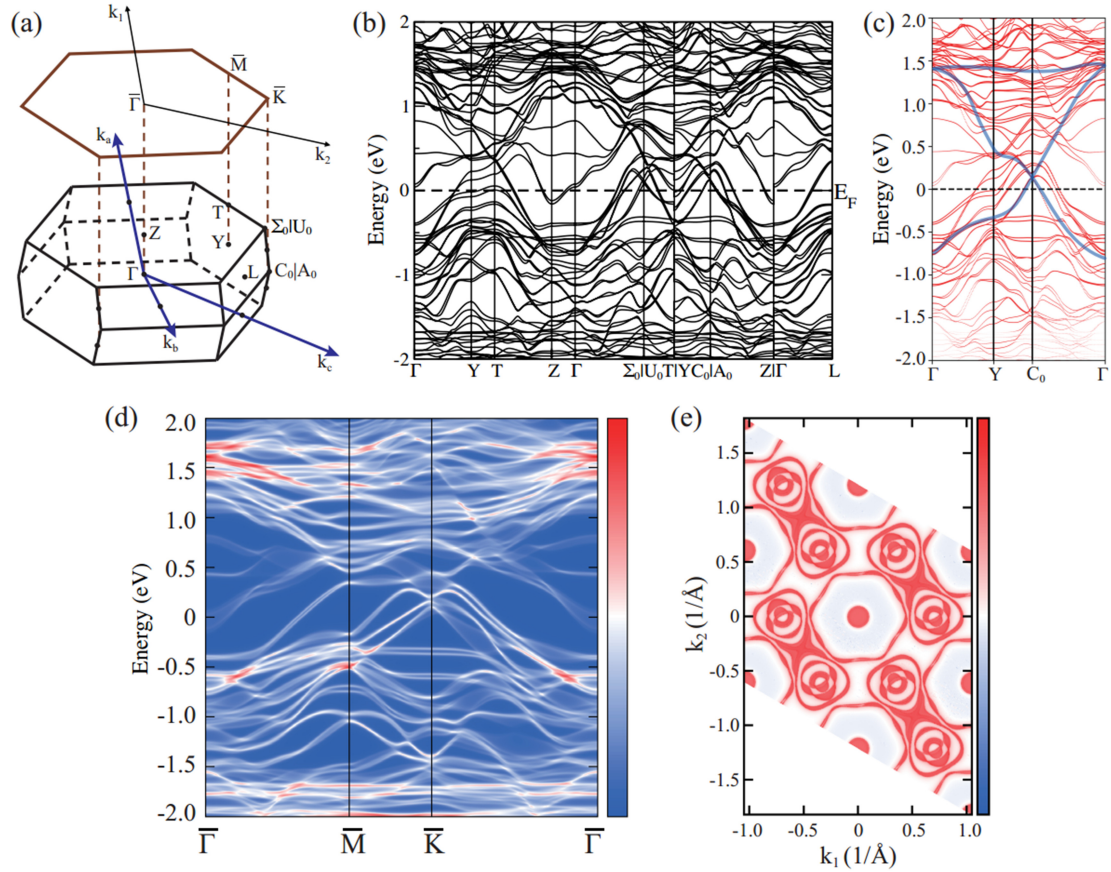


Fig. 4. Electronic structures calculations. (a) The first Brillouin zone (BZ) and two-dimensional projected surface of EuTi_3Bi_4 . (b) The bulk band structure of EuTi_3Bi_4 with SOC ($U=6$ eV). (c) The band projection contributed by $3d$ orbitals of Ti atoms forming the kagome sublattice. The blue lines represent a schematic of the typical bands resulting from the kagome structure. (d-e) The surface states from bulk part (d) and the corresponding Fermi surface (e) on the two-dimensional projected surface of EuTi_3Bi_4 with SOC ($U = 6$ eV).

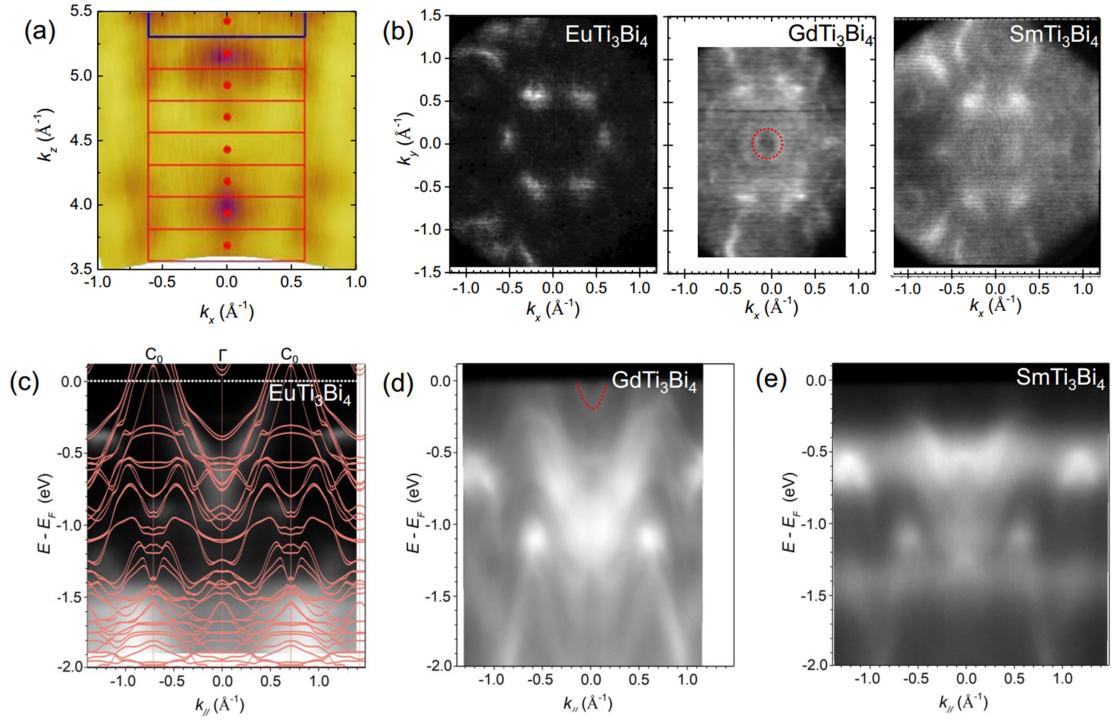


Fig. 5. ARPES measurements. (a) constant energy contours near Fermi energy of SmTi_3Bi_4 in $k_z - k_x$ plane. (b) Fermi pocket morphology of EuTi_3Bi_4 (left), GdTi_3Bi_4 (middle), and SmTi_3Bi_4 (right), (c-e) band dispersion along C_0 - Γ - C_0 direction of (e) EuTi_3Bi_4 (f) GdTi_3Bi_4 and (g) SmTi_3Bi_4 measured with photon energy of 100 eV. All of the spectra are collected at the temperature of 20 K.